Editors' Suggestion

Magnetophotoluminescence of exciton Rydberg states in monolayer WSe_2

Erfu Liu,[1] Jeremiah van Baren,[1] Takashi Taniguchi,[2] Kenji Watanabe,[2] Yia-Chung Chang,[3] and Chun Hung Lui[1,*]

[1]*Department of Physics and Astronomy, University of California, Riverside, California 92521, USA*

[2]*National Institute for Materials Science, Tsukuba, Ibaraki 305-004, Japan*

[3]*Research Center for Applied Sciences, Academia Sinica, Taipei 11529, Taiwan*

(Received 7 March 2019; revised manuscript received 23 April 2019; published 16 May 2019)

Monolayer WSe_2 hosts a series of exciton Rydberg states denoted by the principal quantum number $n = 1, 2, 3$, etc. While most research focuses on their absorption properties, their optical emission is also important but much less studied. Here we measure the photoluminescence from the 1*s*–5*s* exciton Rydberg states in ultraclean monolayer WSe_2 encapsulated by boron nitride under magnetic fields from −31 to 31 T. The exciton Rydberg states exhibit similar Zeeman shifts but distinct diamagnetic shifts from each other. From their luminescence spectra, Zeeman shifts, and diamagnetic shifts, we deduce the binding energies, *g* factors, and radii of the 1*s*–4*s* exciton states. Our results are consistent with theoretical predictions and results from prior magnetoabsorption experiments.

DOI: 10.1103/PhysRevB.99.205420

I. INTRODUCTION

Monolayer transition-metal dichalcogenides (TMDs), such as MoS_2 and WSe_2, possess strong Coulomb interactions due to the reduced dielectric screening and strong spatial confinement in strictly two-dimensional (2D) systems [1–3]. Their electrons and holes can form excitons with binding energies exceeding 100 meV, an order of magnitude larger than those in traditional quasi-2D quantum-well systems [4–16]. The strong interaction produces a series of internal exciton states, which mimic the Rydberg states in the hydrogen atom. They can likewise be characterized by the principal quantum number ($n = 1, 2, 3 \ldots$) and the *s*, *p*, *d* orbitals with quantized angular momentum [Fig. 1(a)] [6–9,17–20]. The exciton Rydberg states in monolayer TMDs possess many remarkable properties, such as nonlocal screening [17], nonhydrogenic spectrum [8], superior valley polarization and coherence [21], strong two-photon coupling [6,9,22], and ultrafast photoresponse [23]. These distinctive properties have stimulated much scientific interest in the research of 2D excitons.

The exciton Rydberg states in monolayer TMDs have been commonly studied with absorption and reflection spectroscopy [7–9,18,24,25]. Although these prior studies reveal many interesting physics of 2D excitons, they mainly focus on the absorption properties. The other aspect of the exciton Rydberg states – the optical emission – is also important, but much less explored experimentally. This is because high-lying exciton levels have short lifetime and weak oscillator strength, leading to tiny optical emission. Ultraclean samples and sensitive measurement are necessary to reveal the fine optical emission from the high-lying exciton levels [20,21,26]. As magnetic field can strongly modify the exciton properties, it is particularly interesting to study the optical emission of exciton Rydberg states under strong magnetic field. However, such experimental studies of 2D exciton magnetoluminescence have been lacking thus far.

In this paper, we measure the photoluminescence (PL) of exciton Rydberg states in ultraclean monolayer WSe_2 encapsulated by boron nitride (BN) under magnetic fields from $B =$ –31 to 31 T. We observe light emission from five (1*s*–5*s*) exciton Rydberg states. From the PL spectra, we can accurately extract the Zeeman shifts and diamagnetic shifts of the 1*s*–4*s* states and further deduce their *g* factors, exciton radii, and binding energies. The results can be quantitatively simulated by a model calculation based on nonhydrogenic excitonic interaction with nonlocal screening in a 2D system embedded in three-dimensional (3D) medium. Our magneto-PL experiment complements prior magnetoabsorption experiments [24] and provides important information to elucidate the diverse properties of exciton Rydberg states in 2D materials.

II. RESULTS AND DISCUSSION

Our experiment was conducted in a 31-T cryogenic magneto-optical system in the National High Magnetic Field Laboratory in Tallahassee, Florida. We measured the PL from BN-encapsulated monolayer WSe_2 at temperature near $T = 4$ K [Fig. 1(b)]. The sample was mounted on a three-dimensional attocube piezoelectric translational stage. A 532-nm continuous laser was directed through a single-mode optical fiber and focused by a lens (numerical aperture = 0.67) onto the sample. The spot diameter on the sample was ∼2 μm. Relatively high incident laser power (∼1 mW) was applied to reveal the weak PL signals from the high-lying exciton states. The PL was collected through a 50/50 beam splitter into a multimode optical fiber, and subsequently measured by a spectrometer (Princeton Instruments, IsoPlane 320) with a charge-coupled device camera. A quarter-wave plate and a linear polarizer were used to select the right-handed circularly polarized component of the PL signal, which corresponds to the emission from the *K* valley in monolayer WSe_2.

*joshua.lui@ucr.edu

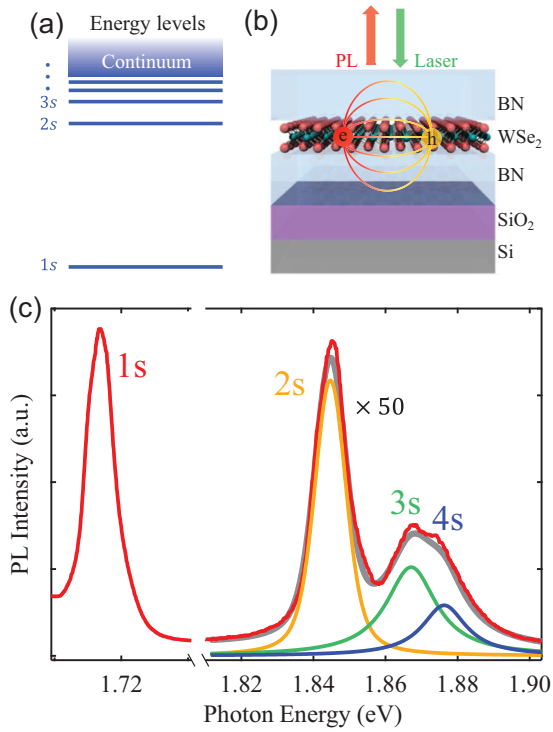

FIG. 1. (a) Schematic internal energy levels of an exciton in monolayer WSe_2. (b) Schematic diagram of an exciton in monolayer WSe_2 encapsulated by BN. The electric field (lines) between the electron (e) and hole (h) spreads into the surrounding BN medium. (c) PL spectrum of monolayer WSe_2 at temperature $T = 4$ K and zero magnetic field under 532-nm continuous laser excitation. The spectrum at 1.81–1.90 eV is multiplied by 50 times for clarity. The red line is the experimental spectrum; the orange, green, and blue lines are the Lorentzian fits to reveal the 2s, 3s, and 4s exciton states, respectively. The gray line is the total fit spectrum.

Figure 1(c) displays a representative PL spectrum of monolayer WSe_2 with no magnetic field. Our ultraclean samples exhibit remarkably sharp PL lines. We can identify the 1s, 2s, 3s, and 4s states of A exciton, which have PL energies (E_{PL}) of 1.712, 1.843, 1.864, and 1.873 eV, respectively (Table I). From the data we extrapolate a free-particle band gap of $E_g = 1.884$ eV by using a quantitative model, which will be described later. The thus-obtained binding energies ($E_b = E_g - E_{PL}$) of 1s–4s excitons are 172, 41, 20, and 11 meV, respectively (Table I). These binding energies are comparable to those of prior absorption experiments on similar BN-encapsulated monolayer WSe_2 samples (see the comparison in Fig. 4) [24]. We only consider the A exciton in this paper. The B exciton of WSe_2, being ~400 meV higher, is well separated from the Rydberg series of the A exciton.

To further explore the A-exciton Rydberg states, we apply strong out-of-plane magnetic field on our samples. Figures 2(a) and 2(c) display the PL maps and cross-cut spectra of monolayer WSe_2 at $B = -31$ to 31 T. The application of magnetic field significantly shifts the energies of all exciton peaks. The high-lying states shift much more than the low-lying states. The resultant enlarged separation between adjacent peaks helps us distinguish different exciton states. In particular, the 4s state, which appears only as a shoulder of the 3s peak at zero field, becomes isolated and well recognized at high magnetic field. To further enhance the weak features, we take the second energy derivative of the PL spectra (d^2I/dE^2) [Figs. 2(b) and 2(d)]. In the d^2I/dE^2 map, the exciton states appear as dips. All the exciton features are sharpened and their energy shifts become more traceable. Remarkably, a PL feature appears above the 4s state at $B > 5$ T. This feature is weak but discernible; it corresponds to the 5s state [Fig. 2(b)]. Besides, we observe a small PL feature at 1.85–1.86 eV above the 2s state [marked by the open dots in Figs. 2(c) and 2(d)]. It shifts parallelly with the 2s state with the magnetic field. The origin of this PL feature is unknown and requires further investigation.

The high-lying (2s–4s) excitons exhibit reduced PL intensity at high magnetic field (Fig. 2). This contrasts with prior absorption experiments, in which the high-lying excitons exhibit enhanced absorption at high magnetic field [24,25]. We can understand the difference by considering the exciton oscillator strength and lifetime. The magnetic field can enhance the exciton oscillator strength because the field can effectively confine an exciton and reduce its spatial size. This effect is particularly prominent for high-lying Rydberg excitons due to their larger spatial size, as observed in the magnetoabsorption experiments [24,25]. However, the magnetic field can also upshift the exciton energy and reduce its lifetime. This effect is also prominent for high-lying excitons due to their large energy upshift. The exciton PL intensity is roughly proportional to the product of oscillator strength and lifetime. Our observation of reduced PL intensity in the 2s–4s states suggests that the reduction of their lifetime overrides the enhancement of oscillator strength under high magnetic field.

We next discuss the magnetic-field dependence of the exciton energy. Figure 3(a) displays the energy of all exciton PL features as a function of magnetic field. According to prior research, the magnetic-field-dependent exciton energy shift consists of two components – the valley Zeeman shift [27–32] and the diamagnetic shift [24,33]. The Zeeman shift is an odd function of B field. The difference between the energies at

TABLE I. PL energy (E_{PL}), binding energy (E_b), g-factor, diamagnetic coefficient (σ), and root-mean-square radius (r) of the exciton Rydberg states in BN-encapsulated monolayer WSe_2. The numbers in parentheses are the theoretical values from our model.

	E_{PL} (eV)	E_b (meV)	g	σ (μeV/T^2)	r (nm)
1s	1.712	172 (172.1)	-4.38 ± 0.12	0.24 ± 0.1 (0.31)	1.6 ± 0.4 (1.68)
2s	1.843	41 (43.8)	-4.60 ± 0.10	6.4 ± 0.2 (4.86)	8.24 ± 0.13 (6.66)
3s	1.864	20 (19.5)	-4.22 ± 0.14	27.3 ± 1.3 (24.2)	17.0 ± 0.4 (14.86)
4s	1.873	11 (11.0)	-5.06 ± 0.21	53.7 ± 3.0 (76.3)	27.8 ± 0.7 (26.37)

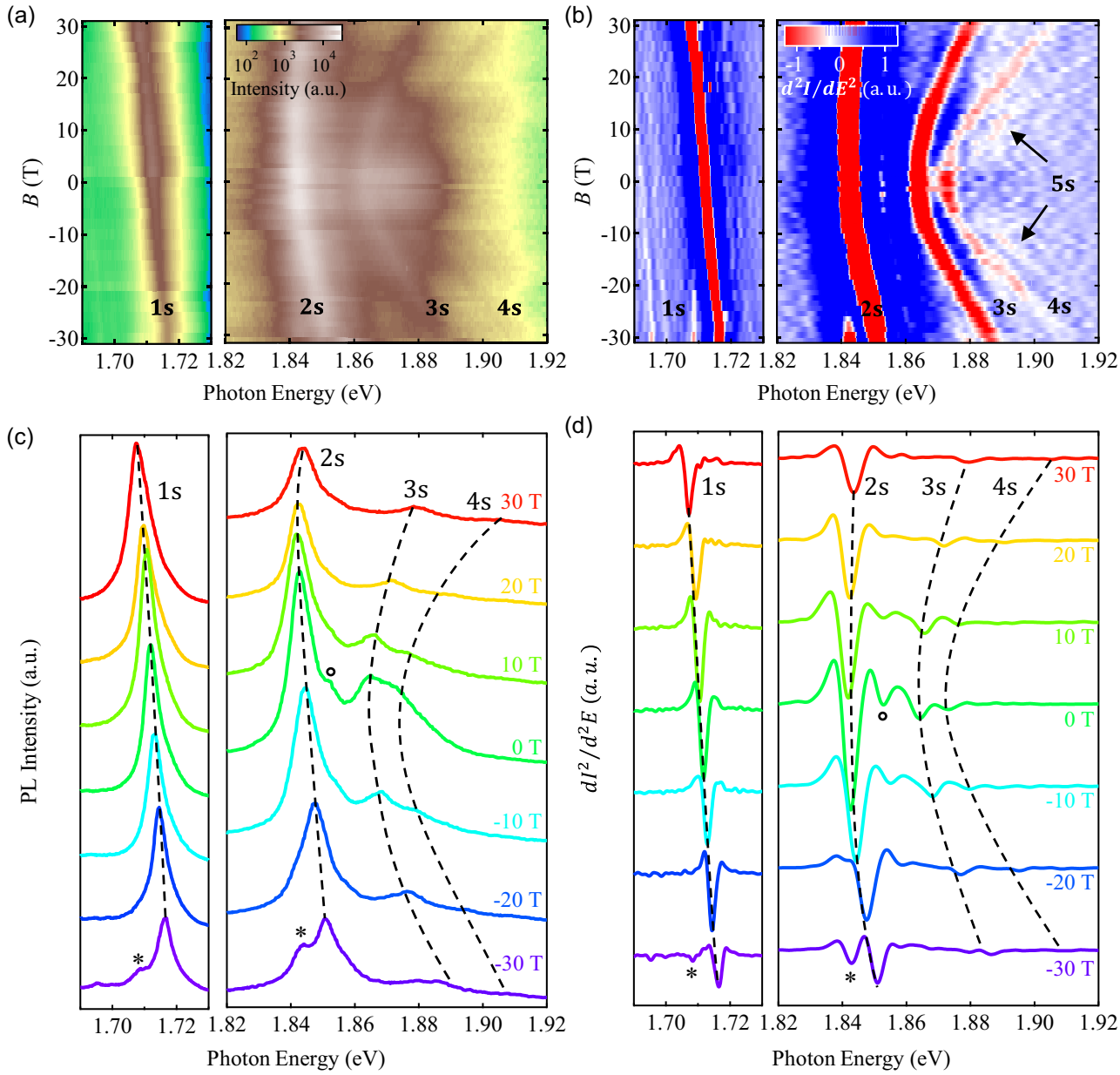

FIG. 2. PL of A-exciton Rydberg states in monolayer WSe_2 under magnetic field at temperature $T = 4$ K. (a) Logarithmic PL maps at magnetic fields $B = -31$ to 31 T. (b) Color map of the second energy derivative of PL intensity (d^2I/dE^2) in panel (a). (c) Cross-cut PL spectra from panel (a) at selective magnetic fields. (d) The cross-cut d^2I/dE^2 spectra from panel (b) at selective magnetic fields. The dashed lines highlight the shift of Rydberg states. PL features marked by the "*" symbol at $B = -30$ T come from the other valley due to the imperfect helicity selection in the measurement.

opposite B fields corresponds to the Zeeman splitting energy. By contrast, the diamagnetic shift is an even function of B field. The average of the energies at opposite B fields corresponds to the diamagnetic shift. We have extracted the Zeeman splitting energies and diamagnetic shifts of the 1s–4s states from our PL data [Figs. 3(b) and 3(c)]. The corresponding shifts of the 5s peak cannot be extracted accurately due to its weak PL signal.

We first consider the Zeeman effect. Prior research has shown that out-of-plane magnetic field can lift the valley degeneracy in monolayer TMDs [27–29,32]. Due to the opposite spin and orbital configurations of the two time-reversal valleys, the magnetic field can enlarge the band gap at one valley but diminish the band gap at the other valley. The difference between the energy gaps of the two valleys is the valley Zeeman (ZM) splitting energy, which can be expressed as

$$\Delta E_{\mathrm{ZM}} = g\mu_{\mathrm{B}}B. \tag{1}$$

Here g is the effective g-factor and $\mu_{\mathrm{B}} = 5.788 \times 10^{-5}$ eV/T is the Bohr magneton. As the Zeeman shift is an odd function of B field, the Zeeman splitting energy can be

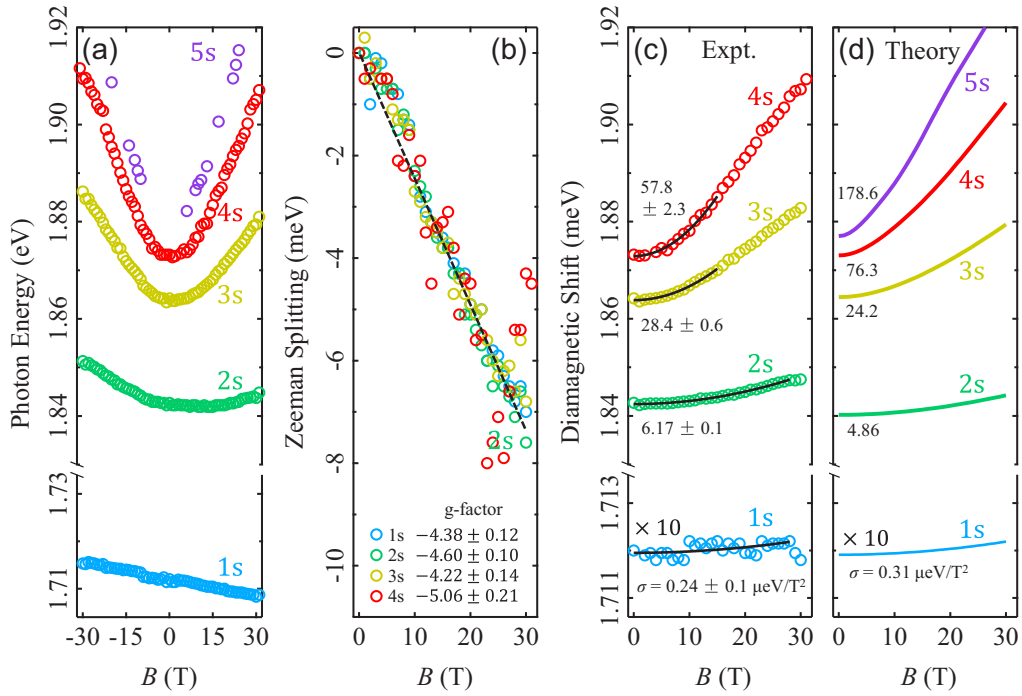

FIG. 3. (a) Exciton PL energy as a function of magnetic field, as extracted from the data in Fig. 2. (b) Zeeman shifts extracted from panel (a). The g factors are obtained from linear fits. (c) Diamagnetic shifts extracted from panel (a). The lines are quadratic fits. (d) Predicted exciton diamagnetic shifts from our model. The y-axis scale of the $1s$ state in panels (c) and (d) is magnified by 10 times for clarify. The numbers denote the measured and calculated diamagnetic coefficient (σ) in unit of $\mu\text{eV/T}^2$.

obtained as the difference between the valley PL energies at opposite B fields. For the bright A exciton with spin singlet, the zero total spin causes no Zeeman shift. The major contribution has been argued to come from the d-type atomic orbitals in the valence band, which has opposite azimuthal quantum numbers $m = +2$ and -2 and opposite magnetic moment at the two valleys [27–29,32]. They contribute an effective g factor of -4 to the valley Zeeman splitting. In our experiment, the Zeeman splitting energies of $1s$–$4s$ states all exhibit linear dependence with g factors between -4.2 and -5.1 [Fig. 3(b); Table I). The results roughly match our simple estimate and prior experiments [27–29,32].

We next consider the diamagnetic shift. In the weak-field limit, where the Landau-level spacing is much smaller than the exciton binding energy, the diamagnetic (DM) shift of an exciton can be expressed as [24,33,34]

$$\Delta E_{\text{DM}} = \frac{e^2}{8\mu}\langle r^2\rangle B^2 = \sigma B^2. \tag{2}$$

Here $\mu = (m_e^{-1} + m_h^{-1})^{-1}$ is the exciton's reduced mass; σ is the diamagnetic coefficient; r is the radial coordinate of the exciton; $\langle r^2\rangle = \langle\psi|r^2|\psi\rangle$ is the expectation value of r^2 over the exciton envelope wave function ψ. The exciton's root-mean-square radius is $r = \sqrt{\langle r^2\rangle} = \sqrt{8\mu\sigma}/e$. A larger diamagnetic shift indicates a larger exciton size. The large high-lying excitons can exhibit much larger diamagnetic shifts than the small low-lying excitons.

In the strong-field limit, where the Landau-level spacing exceeds the exciton binding energy, the optical transition mainly occurs between the Landau levels in the valence and conduction bands. In this regime, the transition energy increases approximately linearly with B as $(N + \frac{1}{2})\hbar\omega_c$ for all exciton states ($\omega_c = eB/\mu$ is the exciton cyclotron frequency). In the regime of mediate B field, the exciton energy will gradually transit from the B^2 to B dependence [24,33,35–38].

Figure 3(c) displays the diamagnetic shifts of $1s$–$4s$ exciton states. The $1s$ and $2s$ energy shifts are small with approximate B^2 dependence in the range of our applied magnetic field ($B = 0$–31 T). $B = 31$ T is a weak field for the $1s$ and $2s$ states because of their large binding energies. By using quadratic fits [lines in Fig. 3(c)], we extract their diamagnetic coefficients to be $\sigma_{1s} = 0.24 \pm 0.1\ \mu\text{eV/T}^2$ and $\sigma_{2s} = 6.4 \pm 0.2\ \mu\text{eV/T}^2$. Previous research has determined that the reduced mass of A exciton in monolayer WSe_2 is $\mu = 0.20\, m_e$, where m_e is the free-electron mass [24]. From the relationship $r = \sqrt{8\mu\sigma}/e$, we calculate the exciton root-mean-square radii to be $r_{1s} = 1.6 \pm 0.4$ nm and $r_{2s} = 8.24 \pm 0.13$ nm for the $1s$ and $2s$ states (Table I).

The $3s$ and $4s$ states exhibit B^2 dependence only at $B < 15$ T and gradually transit to linear B-field dependence at $B > 15$ T. $B = 31$ T is an intermediate field for the $3s$ and $4s$ states because their binding energies (10–20 meV) are comparable to the Landau-level spacing ($\hbar\omega_c \approx 18$ meV at $B = 31$ T). By using quadratic fits on the low-field data [lines in Fig. 3(c)], we extract their diamagnetic coefficients to be $\sigma_{3s} = 27.3 \pm 1.3\ \mu\text{eV/T}^2$ and $\sigma_{4s} = 53.7 \pm 3.0\ \mu\text{eV/T}^2$. The corresponding exciton root-mean-square radii are $r_{3s} = 17.0 \pm 0.4$ nm and $r_{4s} = 27.8 \pm 0.7$ nm. Table I and Fig. 4 summarize the extracted exciton radii of $1s$–$4s$ states. Our results agree with prior magnetoabsorption experiments, which measured the exciton radii of $1s$–$3s$ states (no $4s$ state) in monolayer WSe_2 [24].

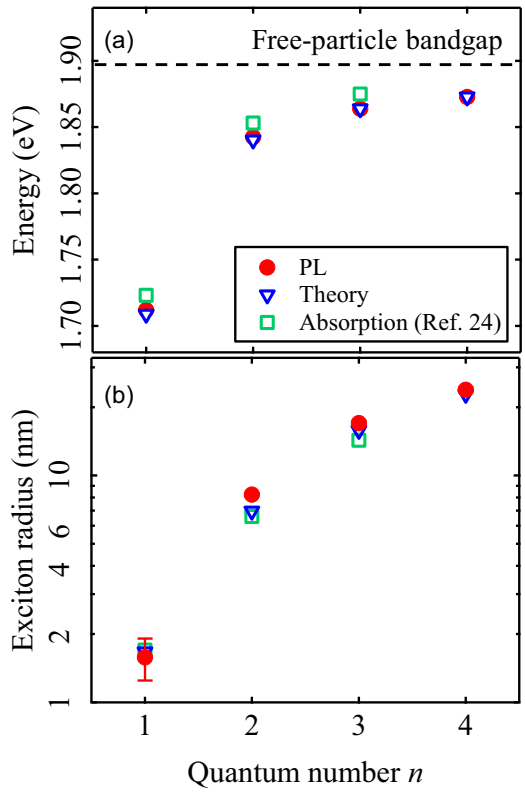

FIG. 4. Energies and radii of Rydberg excitons in monolayer WSe_2 encapsulated by boron nitride. (a) The recombination energy and (b) radii of A-exciton states (red dots) extracted from the PL data in Fig. 3, in comparison with the theoretical predictions (blue triangles) and results from a prior absorption experiment (green squares; Ref. [24]). The dashed line denotes the predicted free-particle band gap by our model.

III. QUANTITATIVE MODEL CALCULATIONS

We have carried out comprehensive model calculations to quantitatively explain our data. We consider a 2D semiconductor (dielectric constant $\varepsilon_{1L-WSe_2} \approx 7.5$) [39] embedded in the 3D medium of boron nitride with lower dielectric constant $\varepsilon_{BN} \approx 3.8$ [39]. In this system, the electrons and holes are confined in a plane, but the electric field between them can extend into the surrounding medium [Fig. 1(b)]. When the electron and hole move away from each other, the portion of outside electric field increases and the total screening becomes weaker. Such nonlocal screening causes the electron-hole interaction to deviate from Coulomb's law. Their interaction potential can be approximated by the Keldysh potential [8,16,40–47]:

$$V(r) = -\frac{e^2}{8\varepsilon_0 r_0}\left[H_0\left(\frac{\kappa r}{r_0}\right) - N_0\left(\frac{\kappa r}{r_0}\right)\right]. \quad (3)$$

Here H_0 and N_0 are the Struve and Neuman functions of zeroth order, respectively; r is the electron-hole distance; r_0 is an effective screening length of monolayer WSe_2; κ is the effective static dielectric constant of the heterostructure. Both r_0 and κ are fitting parameters in our model. The Keldysh potential considers the nonlocal screening effect of the embedded 2D system. In the long-range limit ($r \gg r_0$), $V(r)$ scales as $1/\kappa r$ due to the vanishing screening from WSe_2. In the short-range limit ($r \ll r_0$), $V(r)$ diverges only weakly as $\log(r)$ due to the increased screening from WSe_2.

We have used the Keldysh potential to calculate the energies of exciton Rydberg states in BN-encapsulated monolayer WSe_2 under varying magnetic field. Our calculation uses the effective mass of electron and hole extracted from the density-functional theory (DFT). We obtain the best-fit parameters $r_0 = 5$ nm and $\kappa = 3.97$ by adjusting their values within the physical range to fit the observed exciton energies. Our calculation predicts a free-particle band gap of 1.884 eV for BN-encapsulated monolayer WSe_2. Figures 4(a) and 4(b) display our calculated recombination energies and radii of the $1s$–$4s$ exciton states. They agree excellently with the experimental results. We have also calculated the diamagnetic shifts of the $1s$–$5s$ states [Fig. 3(d)]. The calculation quantitatively reproduces the observed diamagnetic shifts in experiment.

IV. CONCLUSION

We have investigated the exciton Rydberg series of ultraclean monolayer WSe_2 by magnetic-field-dependent photoluminescence. We observe the PL from the $1s$–$5s$ exciton states. We extract the binding energies, g factor, and radii of the $1s$–$4s$ excitons from their PL spectra, Zeeman shifts, and diamagnetic shifts. Compared to prior reflection experiments that involve optical interference in stacked materials on the Si/SiO_2 substrates, our magneto-PL experiment and analysis are more straightforward to implement. Moreover, our PL measurement appears to be more sensitive than previous experiments. We can reveal the $5s$ state and the full range of diamagnetic shifts of the $4s$ state, which were not observed in prior experiments. Overall, our research demonstrates magneto-PL to be an efficient and powerful method to investigate the exciton Rydberg states in 2D semiconductors. Our PL results also provide key information for optical and optoelectronic applications of TMD materials.

Note added. We recently became aware of two similar papers on the magnetophotoluminescence of monolayer WSe_2 [25,26].

ACKNOWLEDGMENTS

Y.-C.C. is supported by Ministry of Science and Technology (Taiwan) under Grant No. MOST 107-2112-M-001-032. K.W. and T.T. acknowledge support from the Elemental Strategy Initiative conducted by the MEXT, Japan and the CREST (Grant No. JPMJCR15F3), JST. We thank Dmitry Smirnov and Zhengguang Lu for assistance in the magneto-optical experiment.

APPENDIX: THEORETICAL CALCULATION OF EXCITON RYDBERG STATES IN MONOLAYER WSe_2

The band structure of monolayer WSe_2 near the K (or K') point is nearly parabolic for both the conduction and valence bands [4,48,49]. The electron and hole effective masses are estimated to be around $0.38m_e$ and $0.44m_e$ (m_e is the free-electron mass), respectively, according to the average values of various calculations based on the DFT [4,48–50]. So,

the reduced mass (μ) for the exiton in monolayer WSe_2 is around $0.2m_e$. The effective electron-hole interaction in 2D transition-metal dichalcogenides encapsulated in boron nitride can be approximated by a quasi-2D potential of the following form in the momentum space: [8,42–46]:

$$V(q) = -\frac{e^2}{2A\kappa\varepsilon_0 q(1+q\rho_0)}. \tag{A1}$$

Here A is the sample area; κ is the effective static dielectric constant of the heterostructure; ρ_0 is an empirical parameter related to the finite thickness of the 2D material and the screening length of the q-dependent dielectric screening [51]. The band-structure effect can lead to another q-dependent factor [52], which can also be absorbed into the parameter ρ_0. The Fouier transform of $V(q)$ takes the following form in the real space:

$$V(r) = -\frac{e^2}{8\varepsilon_0 r_0}\left[H_0\left(\frac{\kappa r}{r_0}\right) - N_0\left(\frac{\kappa r}{r_0}\right)\right]. \tag{A2}$$

Here r is radial coordinate in two dimensions; H_0 and N_0 are the Struve and Neuman functions of zeroth order, respectively. In the spherical effective-mass approximation, the Hamiltonian for the electron-hole relative motion in the exciton is

$$H_X = -\frac{\hbar^2\nabla^2}{2\mu} + V(r). \tag{A3}$$

The eigenvalues of the low-lying states can be obtained via the Rayleigh-Ritz variational method [53,54] with a finite basis set of localized functions. The basis functions for the s-like states take the exponential form:

$$f_n(r) = C_n e^{-\alpha_n r}. \tag{A4}$$

The exponents α_n follow an even-tempered series $\alpha_n = \alpha g^n$ $(n = 0, \ldots, N-1)$. $C_n = 2\alpha_n/\sqrt{2\pi}$ is the normalization constant. α and g are variational parameters to minimize the eigenvalues of the low-lying states. In our calculation, we choose $\alpha = 0.025$, $g = 1.4$, and $N = 15$. The basis set is then orthogonalized via the Gram-Schmid procedure. We adopt an effective dielectric constant $\kappa = 3.97$. The corresponding atomic unit for exciton energy is $R_X = (\mu/\kappa^2)\,13.6\,\text{eV} = 0.172\,\text{eV}$ and the atomic unit for distance is $a_X = (\kappa/\mu)\,0.529\,\text{Å} = 10.5\,\text{Å}$. We found that, by using $\kappa = 3.97$ and $r_0/\kappa = 1.2\,a_X$, the model potential can describe well the measured energy levels of the five lowest-lying excitonic states in monolayer WSe_2. Both parameters are physically reasonable and close to the values considered in Ref. [46].

After diagonalizing the Hamiltonian H_X (A3) within the orthogonalized basis set, we obtain the five lowest-lying eigenstates. To check the suitability of the basis set, we also diagonalize the Hamiltonian for the ideal 2D exciton (by setting $\rho_0 = 0$) within the same basis set. The resultant eigenvalues agree with the exact values given by $R_X/(n-1/2)^2$ with error smaller than $2 \times 10^{-6} R_X$ for the four lowest-lying eigenstates and smaller than $2 \times 10^{-5} R_X$ for the fifth eigenstate.

To describe the diamagnetic shift of the excitonic states, we consider the effect of a constant magnetic field (B) perpendicular to the 2D material by the following Hamiltonian: [55]

$$H = \frac{1}{2\mu}(\boldsymbol{p} + e\boldsymbol{A})^2 + V = \frac{1}{2\mu}\left(p^2 + 2e\boldsymbol{p}\cdot\boldsymbol{A} + e^2A^2\right) + V, \tag{A5}$$

where

$$\boldsymbol{A} = \tfrac{1}{2}\boldsymbol{B}\times\boldsymbol{r}, \tag{A6}$$

$$A^2 = \tfrac{1}{4}r^2B^2, \tag{A7}$$

$$\boldsymbol{p}\cdot\boldsymbol{A} = \tfrac{1}{2}\boldsymbol{B}\cdot(\boldsymbol{r}\times\boldsymbol{p}) = \tfrac{1}{2}\boldsymbol{B}\cdot\boldsymbol{L}. \tag{A8}$$

For s-like states, the zero angular momentum ($\boldsymbol{L}$) makes $\boldsymbol{p}\cdot\boldsymbol{A} = 0$. The Hamiltonian becomes $H = H_X + H_{\text{DM}}$, where H_{DM} is the diamagnetic term:

$$H_{\text{DM}} = \frac{e^2}{8\mu}r^2B^2. \tag{A9}$$

The first-order perturbation theory gives the diamagnetic shift of the exciton energy level:

$$\Delta E_{\text{DM}} = \frac{e^2}{8\mu}\langle r^2\rangle B^2 = \sigma B^2. \tag{A10}$$

Here $\langle r^2\rangle = \langle\psi|r^2|\psi\rangle$ is the expectation value of r^2 over the exciton envelope wave function ψ. The exciton's root-mean-square radius is $r = \sqrt{\langle r^2\rangle} = \sqrt{8\mu\sigma}/e$.

The first-order perturbation theory gives good approximation only in the low field. In the full calculation, we have calculated the exact diamagnetic shift by diagonalizing the total Hamiltonian $H = H_X + H_{\text{DM}}$ for each magnetic field. We note that, as the H_{DM} term behaves like a parabolic confining potential, the exciton size will shrink when the magnetic field increases. The calculated exciton sizes in the main text are the values in the weak-field limit.

[1] L. Britnell, R. Ribeiro, A. Eckmann, R. Jalil, B. Belle, A. Mishchenko, Y.-J. Kim, R. Gorbachev, T. Georgiou, and S. Morozov, Strong light-matter interactions in heterostructures of atomically thin films, Science **340**, 1311 (2013).

[2] K. F. Mak, C. Lee, J. Hone, J. Shan, and T. F. Heinz, Atomically Thin MoS: A New Direct-Gap Semiconductor, Phys. Rev. Lett. **105**, 136805 (2010).

[3] A. Splendiani, L. Sun, Y. Zhang, T. Li, J. Kim, C.-Y. Chim, G. Galli, and F. Wang, Emerging photoluminescence in monolayer MoS_2, Nano Lett. **10**, 1271 (2010).

[4] A. Ramasubramaniam, Large excitonic effects in monolayers of molybdenum and tungsten dichalcogenides, Phys. Rev. B **86**, 115409 (2012).

[5] D. Y. Qiu, F. H. da Jornada, and S. G. Louie, Optical Spectrum of MoS_2: Many-Body Effects and Diversity of Exciton States, Phys. Rev. Lett. **111**, 216805 (2013).

[6] G. Wang, X. Marie, I. Gerber, T. Amand, D. Lagarde, L. Bouet, M. Vidal, A. Balocchi, and B. Urbaszek, Giant Enhancement of the Optical Second-Harmonic Emission of WSe_2 Monolayers by Laser Excitation at Exciton Resonances, Phys. Rev. Lett. **114**, 097403 (2015).

[7] K. He, N. Kumar, L. Zhao, Z. Wang, K. F. Mak, H. Zhao, and J. Shan, Tightly Bound Excitons in Monolayer WSe_2, Phys. Rev. Lett. **113**, 026803 (2014).

[8] A. Chernikov, T. C. Berkelbach, H. M. Hill, A. Rigosi, Y. Li, O. B. Aslan, D. R. Reichman, M. S. Hybertsen, and T. F. Heinz, Exciton Binding Energy and Nonhydrogenic Rydberg Series in Monolayer WS_2, Phys. Rev. Lett. **113**, 076802 (2014).

[9] Z. Ye, T. Cao, K. O'Brien, H. Zhu, X. Yin, Y. Wang, S. G. Louie, and X. Zhang, Probing excitonic dark states in single-layer tungsten disulphide, Nature (London) **513**, 214 (2014).

[10] C. Zhang, A. Johnson, C.-L. Hsu, L.-J. Li, and C.-K. Shih, Direct imaging of band profile in single layer MoS_2 on graphite: Quasiparticle energy gap, metallic edge states, and edge band bending, Nano Lett. **14**, 2443 (2014).

[11] M. M. Ugeda, A. J. Bradley, S.-F. Shi, F. H. da Jornada, Y. Zhang, D. Y. Qiu, W. Ruan, S.-K. Mo, Z. Hussain, Z.-X. Shen, F. Wang, S. G. Louie, and M. F. Crommie, Giant bandgap renormalization and excitonic effects in a monolayer transition metal dichalcogenide semiconductor, Nat. Mater. **13**, 1091 (2014).

[12] G. Wang, A. Chernikov, M. M. Glazov, T. F. Heinz, X. Marie, T. Amand, and B. Urbaszek, Colloquium: Excitons in atomically thin transition metal dichalcogenides, Rev. Mod. Phys. **90**, 021001 (2018).

[13] A. T. Hanbicki, M. Currie, G. Kioseoglou, A. L. Friedman, and B. T. Jonker, Measurement of high exciton binding energy in the monolayer transition-metal dichalcogenides WS_2 and WSe_2, Solid State Commun. **203**, 16 (2015).

[14] T. Cheiwchanchamnangij and W. R. L. Lambrecht, Quasiparticle band structure calculation of monolayer, bilayer, and bulk MoS_2, Phys. Rev. B **85**, 205302 (2012).

[15] F. Hüser, T. Olsen, and K. S. Thygesen, How dielectric screening in two-dimensional crystals affects the convergence of excited-state calculations: Monolayer MoS_2, Phys. Rev. B **88**, 245309 (2013).

[16] T. C. Berkelbach, M. S. Hybertsen, and D. R. Reichman, Theory of neutral and charged excitons in monolayer transition metal dichalcogenides, Phys. Rev. B **88**, 045318 (2013).

[17] A. Chernikov, A. M. van der Zande, H. M. Hill, A. F. Rigosi, A. Velauthapillai, J. Hone, and T. F. Heinz, Electrical Tuning of Exciton Binding Energies in Monolayer WS_2, Phys. Rev. Lett. **115**, 126802 (2015).

[18] H. M. Hill, A. F. Rigosi, C. Roquelet, A. Chernikov, T. C. Berkelbach, D. R. Reichman, M. S. Hybertsen, L. E. Brus, and T. F. Heinz, Observation of excitonic Rydberg states in monolayer MoS_2 and WS_2 by photoluminescence excitation spectroscopy, Nano Lett. **15**, 2992 (2015).

[19] B. Zhu, X. Chen, and X. Cui, Exciton binding energy of monolayer WS_2, Sci. Rep. **5**, 9218 (2015).

[20] B. Han, C. Robert, E. Courtade, M. Manca, S. Shree, T. Amand, P. Renucci, T. Taniguchi, K. Watanabe, X. Marie, L. E. Golub, M. M. Glazov, and B. Urbaszek, Exciton States in Monolayer $MoSe_2$ and $MoTe_2$ Probed by Upconversion Spectroscopy, Phys. Rev. X **8**, 031073 (2018).

[21] S.-Y. Chen, T. Goldstein, J. Tong, T. Taniguchi, K. Watanabe, and J. Yan, Superior Valley Polarization and Coherence of 2s Excitons in Monolayer WSe_2, Phys. Rev. Lett. **120**, 046402 (2018).

[22] T. C. Berkelbach, M. S. Hybertsen, and D. R. Reichman, Bright and dark singlet excitons via linear and two-photon spectroscopy in monolayer transition-metal dichalcogenides, Phys. Rev. B **92**, 085413 (2015).

[23] A. Klots, A. Newaz, B. Wang, D. Prasai, H. Krzyzanowska, J. Lin, D. Caudel, N. Ghimire, J. Yan, and B. Ivanov, Probing excitonic states in suspended two-dimensional semiconductors by photocurrent spectroscopy, Sci. Rep. **4**, 6608 (2014).

[24] A. V. Stier, N. P. Wilson, K. A. Velizhanin, J. Kono, X. Xu, and S. A. Crooker, Magnetooptics of Exciton Rydberg States in a Monolayer Semiconductor, Phys. Rev. Lett. **120**, 057405 (2018).

[25] M. Goryca, J. Li, A. V. Stier, S. A. Crooker, T. Taniguchi, K. Watanabe, E. Courtade, S. Shree, C. Robert, B. Urbaszek, and X. Marie, Revealing exciton masses and dielectric properties of monolayer semiconductors with high magnetic fields, arXiv:1904.03238.

[26] S.-Y. Chen, Z. Lu, T. Goldstein, J. Tong, A. Chaves, J. Kunstmann, L. S. R. Cavalcante, T. Woźniak, G. Seifert, D. R. Reichman, T. Taniguchi, K. Watanabe, D. Smirnov, and J. Yan, Luminescent emission of excited Rydberg excitons from monolayerWSe_2, Nano Lett. **19**, 2464 (2019).

[27] Y. Li, J. Ludwig, T. Low, A. Chernikov, X. Cui, G. Arefe, Y. D. Kim, A. M. van der Zande, A. Rigosi, H. M. Hill, S. H. Kim, J. Hone, Z. Li, D. Smirnov, and T. F. Heinz, Valley Splitting and Polarization by the Zeeman Effect in Monolayer $MoSe_2$, Phys. Rev. Lett. **113**, 266804 (2014).

[28] G. Aivazian, Z. Gong, A. M. Jones, R.-L. Chu, J. Yan, D. G. Mandrus, C. Zhang, D. Cobden, W. Yao, and X. Xu, Magnetic control of valley pseudospin in monolayerWSe_2, Nat. Phys. **11**, 148 (2015).

[29] D. MacNeill, C. Heikes, K. F. Mak, Z. Anderson, A. Kormányos, V. Zólyomi, J. Park, and D. C. Ralph, Breaking of Valley Degeneracy by Magnetic Field in Monolayer $MoSe_2$, Phys. Rev. Lett. **114**, 037401 (2015).

[30] G. Wang, L. Bouet, M. M. Glazov, T. Amand, E. L. Ivchenko, E. Palleau, X. Marie, and B. Urbaszek, Magneto-optics in transition metal diselenide monolayers, 2D Mater. **2**, 034002 (2015).

[31] A. Arora, R. Schmidt, R. Schneider, M. R. Molas, I. Breslavetz, M. Potemski, and R. Bratschitsch, Valley Zeeman splitting and valley polarization of neutral and charged excitons in monolayer $MoTe_2$ at high magnetic fields, Nano Lett. **16**, 3624 (2016).

[32] A. Srivastava, M. Sidler, A. V. Allain, D. S. Lembke, A. Kis, and A. Imamoğlu, Valley Zeeman effect in elementary optical excitations of monolayer WSe_2, Nat. Phys. **11**, 141 (2015).

[33] A. V. Stier, K. M. McCreary, B. T. Jonker, J. Kono, and S. A. Crooker, Exciton diamagnetic shifts and valley Zeeman effects in monolayer WS_2 and MoS_2 to 65 Tesla, Nat. Commun. **7**, 10643 (2016).

[34] N. Miura, *Physics of Semiconductors in High Magnetic Fields* (Oxford University Press, Oxford, 2007), Vol. 15.

[35] O. Akimoto and H. Hasegawa, Interband optical transitions in extremely anisotropic semiconductors. II. Coexistence of exciton and the Landau levels, J. Phys. Soc. Jpn., **22**, 181 (1967).

[36] A. H. MacDonald and D. S. Ritchie, Hydrogenic energy levels in two dimensions at arbitrary magnetic fields, Phys. Rev. B **33**, 8336 (1986).

[37] W. Edelstein, H. N. Spector, and R. Marasas, Two-dimensional excitons in magnetic fields, Phys. Rev. B **39**, 7697 (1989).

[38] J. Have, G. Catarina, T. G. Pedersen, and N. M. R. Peres, Monolayer transition metal dichalcogenides in strong magnetic fields: Validating the Wannier model using a microscopic calculation, Phys. Rev. B **99**, 035416 (2019).

[39] A. Laturia, M. L. Van de Put, and W. G. Vandenberghe, Dielectric properties of hexagonal boron nitride and transition metal dichalcogenides: From monolayer to bulk, npj 2D Mater. Appl. **2**, 6 (2018).

[40] F. Wu, F. Qu, and A. H. MacDonald, Exciton band structure of monolayer MoS_2, Phys. Rev. B **91**, 075310 (2015).

[41] I. Kylänpää and H.-P. Komsa, Binding energies of exciton complexes in transition metal dichalcogenide monolayers and effect of dielectric environment, Phys. Rev. B **92**, 205418 (2015).

[42] N. S. Rytova, The screened potential of a point charge in a thin film, Moscow Univ. Phys. Bull. **3**, 183 (1967).

[43] L. Keldysh, Coulomb interaction in thin semiconductor and semimetal films, JETP Lett. **29**, 658 (1979).

[44] G. Sanders and Y.-C. Chang, Theory of photoabsorption in modulation-doped semiconductor quantum wells, Phys. Rev. B **35**, 1300 (1987).

[45] R. Y. Kezerashvili and S. M. Tsiklauri, Trion and biexciton in monolayer transition metal dichalcogenides, Few-Body Syst. **58**, 18 (2017).

[46] E. Courtade, M. Semina, M. Manca, M. M. Glazov, C. Robert, F. Cadiz, G. Wang, T. Taniguchi, K. Watanabe, M. Pierre *et al.*, Charged excitons in monolayer WSe_2: Experiment and theory, Phys. Rev. B **96**, 085302 (2017).

[47] D. Van Tuan, M. Yang, and H. Dery, Coulomb interaction in monolayer transition-metal dichalcogenides, Phys. Rev. B **98**, 125308 (2018).

[48] H. Shi, H. Pan, Y.-W. Zhang, and B. I. Yakobson, Quasiparticle band structures and optical properties of strained monolayer MoS_2 and WS_2, Phys. Rev. B **87**, 155304 (2013).

[49] A. Kormányos, B. Burkard, M. Gmitra, J. Fabian, V. Zólyomi, N. D. Drummond, and V. Fal'ko, $k \cdot p$ theory for two-dimensional transition metal dichalcogenide semiconductors, 2D Mater. **2**, 022001 (2015).

[50] I. Filikhin, R. Y. Kezerashvili, S. M. Tsiklauri, and B. Vlahovic, Trions in bulk and monolayer materials: Faddeev equations and hyperspherical harmonics, Nanotechnology **29**, 124002 (2018).

[51] K. S. Thygesen, Calculating excitons, plasmons, and quasiparticles in 2D materials and van der Waals heterostructures, 2D Mater. **4**, 022004 (2017).

[52] G. Berghäuser and E. Malic, Analytical approach to excitonic properties of MoS_2, Phys. Rev. B **89**, 125309 (2014).

[53] W. Ritz, Über eine neue Methode zur Lösung gewisser Variationsprobleme der mathematischen Physik, J. fr die reine und angewandte Mathematik (Crelle's Journal) **1909**, 135 (2009).

[54] J. MacDonald, Successive approximations by the Rayleigh-Ritz variation method, Phys. Rev. **43**, 830 (1933).

[55] B. Stébé, E. Feddi, and G. Munschy, Excitonic trions in a low magnetic field, Phys. Rev. B **35**, 4331 (1987).